environments

MDPI

Article

Identification and Quantification of Dust-Located Environmentally Persistent Free Radicals

Rachid Ismail [1], Mohammednoor Altarawneh [1] and Joy H. Tannous [1,2,*]

[1] Department of Chemical and Petroleum Engineering, United Arab Emirates University, F1 Building, Al-Ain P.O. Box 15551, United Arab Emirates
[2] National Water and Energy Center, United Arab Emirates University, Al-Ain P.O. Box 15551, United Arab Emirates
* Correspondence: j.tannous@uaeu.ac.ae

Abstract

Airborne fine particulate matter ($PM_{2.5}$) has been extensively identified as a major contributor to adverse health outcomes, including respiratory illnesses, cardiovascular diseases, and premature mortality. $PM_{2.5}$ poses an even greater threat due to the presence of environmentally persistent free radicals (EPFRs). It is, thus, important to study human exposure to EPFRs. Dust samples from residential areas in Al Ain, UAE, were tested, and free radicals were detected and quantified. ESR measurements showed distinct signals with g-factors around 2.004–2.006, typically associated with oxygen-centered EPFRs. Spin concentrations were quantified at approximately 2.64×10^{16} spins/g in Dust Sample 1 (DS1) and 2.36×10^{17} spins/g in Dust Sample 2 (DS2), values comparable to those reported in other regions. DS1 and DS2 were collected from two different locations in inhabited areas of the city of Al Ain. Fourier Transform InfraRed (FTIR) spectra revealed possible functional groups such as catechols and hydroquinones, while X-ray diffraction (XRD) confirmed mineral oxides that could stabilize these radicals. However, the spectra also displayed features consistent with the six-line hyperfine splitting of Mn. These findings confirm the presence of environmentally relevant paramagnetic species in dust, which have implications for human health.

Keywords: environmentally persistent free radicals; dust; electron spin resonance; free radical; semi-quinones; manganese

1. Introduction

Airborne fine particulate matter ($PM_{2.5}$) is a well-established environmental and public health concern, linked to respiratory and cardiovascular diseases as well as premature mortality [1–3]. These health effects are largely associated with the toxic constituents of $PM_{2.5}$—such as polycyclic aromatic hydrocarbons (PAHs), heavy metals, and persistent organic pollutants (POPs)—that adsorb onto fine particles and enhance their biological reactivity [4–6]. Despite substantial reductions in ambient $PM_{2.5}$ concentrations in many regions—for instance, a 46% decline in the United States between 2005 and 2024 to approximately 7.5 $\mu g/m^3$—the levels remain above the World Health Organization's 5 $\mu g/m^3$ guideline [7,8].

Beyond its mass concentration, the health relevance of PM is increasingly interpreted through its chemical and redox activities. The Global Burden of Disease 2021 analysis continues to identify particulate air pollution as a major risk factor for premature mortality,

Check for updates

Academic Editors: Peter Brimblecombe and Yanling Deng

Received: 4 June 2026
Revised: 11 July 2026
Accepted: 20 July 2026
Published: 24 July 2026

Copyright: © 2026 by the authors. Licensee MDPI, Basel, Switzerland. This article is an open access article distributed under the terms and conditions of the Creative Commons Attribution (CC BY) license.

while recent EPFR reviews emphasize that persistent radicals are important because they can carry oxidative reactivity across air, dust, soil, and indoor reservoirs [9,10].

Among the various toxic species in $PM_{2.5}$, environmentally persistent free radicals (EPFRs) have emerged as a particularly hazardous class due to their high stability and oxidative potential. Formed primarily during combustion processes (e.g., vehicle emissions, industrial activities, and biomass burning), EPFRs can persist for extended periods because of resonance stabilization on particle surfaces and interactions with redox-active metals such as Fe and Cu [11–19]. These radicals are capable of generating reactive oxygen species (ROS) and inducing oxidative stress, thereby contributing to the toxicity of airborne particulate matter [11–14].

The current state of the art treats EPFRs not as a single compound but as a heterogeneous family of particle-stabilized paramagnetic species, including carbon-centered, oxygen-centered, semiquinone/phenoxy-type, and metal-associated signals. Recent reviews also stress that Electron Spin Resonance (ESR) is the primary direct method for detecting EPFRs, but that interpretation based only on the g-factor can be uncertain in complex environmental matrices; therefore, combining ESR with complementary mineralogical and spectroscopic techniques is increasingly recommended [20–22].

EPFRs have been identified in diverse environments—from heavily polluted urban centers like Beijing to rural regions—indicating their potential for long-range atmospheric susceptibility, as well as their high tendency to occur in organic systems [5,17,23]. EPFRs' occurrence is not limited to ambient air, as they have also been detected in soil, road dust, and indoor environments [19,23–27]. The ubiquity and persistence of these radicals raise concerns about chronic exposure through both inhalation and ingestion of resuspended dust. Organic precursors such as hydroquinones and catechols, which are produced during combustion processes like diesel exhaust, wood burning, and cigarette smoking, are key contributors to the formation of phenolic-type EPFRs [5,11,28–32]. These compounds decompose through thermal reactions, leading to the creation of semiquinone radicals, which are commonly found as EPFRs in ambient PM [19].

Recent experimental work has also shifted attention from outdoor $PM_{2.5}$ alone to indoor particles, settled dust, surface films, and road dust. In a residential indoor case study, EPFRs were detected in airborne PM, dust, and surface samples, and the authors estimated dust and surfaces to be larger contributors to total in-home EPFR abundance than suspended PM [33]. A longitudinal household dust study further reported EPFR detection in more than 95% of samples and suggested that house dust can act as a persistent exposure reservoir, while another recent study associated household ventilation, cooking practices, traffic-related air pollution, and cleaning habits with EPFR concentrations in dust [34,35]. Road dust research has similarly linked EPFRs with oxidative potential, supporting the view that deposited dust is not merely an inert carrier but a chemically reactive exposure medium [36]. It is also noteworthy that the presence of efficient free-radical scavengers of technogenic origin in environmental pollution, derived from cigarette smoke, may represent a certain challenge for toxicology and ecotoxicology in the elucidation of the overall environmental impact of EPFRs and the resulting risk factors for living organisms [37,38].

To understand the true impact of EPFRs on health, it is crucial to measure personal exposure under real-world conditions, taking into account the dynamic nature of exposure in different environments and how it enters the custodian's life through accumulated dust. Measurement of EPFRs typically involves detecting the presence of EPFRs in collected particulate matter, often using techniques such as ESR spectroscopy. In fact, measurements of EPFR content in dust and particulate matter from different countries and cities in the world, including Saudi Arabia, India, China, and the United States of America, have

been reported in the literature [39–42]. In the current work, the high-end ESR apparatus employed allows quantification of the EPFRs, albeit on a spins per gram of PM basis.

While prior research has characterized EPFR formation from combustion sources and their oxidative behavior, several knowledge gaps remain. Most existing studies focus on outdoor aerosols, with limited attention to indoor and settled dust where human exposure can be significant. In addition, only a limited number of studies quantify free radicals' concentration. The novelty of this study lies in the direct detection and quantification of free radicals in indoor and outdoor dust samples from residential areas without solvent extraction or exposure to conditions that could modify their chemical composition. Moreover, extending EPFR research to a new region such as the inhabited desert regions of the UAE was a main goal. Furthermore, unlike the current case at hand, most of the previously researched locations emphasized the role of nearby polluting factors such as factories of different kinds, whereas this study focuses on an inhabited area surrounded by a lifestyle that is predominantly custodian. This combination of a residential Gulf setting, untreated dust collection, and direct ESR-based quantification distinguishes the work from previous EPFR investigations.

The methodology employed in the current work enables an accurate assessment of personal exposure to EPFRs under real-world conditions. Furthermore, the study represents the first investigation of its kind conducted in the Gulf region. The findings have important implications for both environmental and public health. The persistence of these radicals on particulate surfaces—commonly encountered in domestic and urban settings—combined with their capacity to generate reactive oxygen species (ROS), underscores their potential toxicity. By advancing the understanding of EPFR occurrence, composition, and stability in real-world dust, this study provides a foundation for more effective exposure assessments and preventive strategies against EPFR-induced air pollution.

2. Methodology

2.1. Materials

In the current study, testing took place on environmental dust samples. Environmental dust was physically collected without the use of any solvents, additives, pre-treatment, or sieving. The collection was conducted at high-altitude locations on both balconies and windows during the fall season in September, with temperatures of about 38–40 °C, at two locations in Al Ain, Abu Dhabi, United Arab Emirates. An average of around 40 g was collected from each location. Both locations, which are widely separated, represent residential buildings relatively far from industrial areas. They were classified as DS1 and DS2 depending on the area from which they were retrieved. They were stored at room temperature in sealed containers to avoid possible interactions with oxygen in the air. The samples were left unfiltered and unsieved to properly replicate what the human body is exposed to. Further details about the characteristics of DS1 and DS2 are mentioned in Section 3.2. The typical climate of Al Ain is that of a dry region in the middle of the Abu Dhabi desert, which rarely experiences rainfall during the year, and can be regarded as generally uniform.

2.2. Equipment and Procedures

Dust samples were subject to analytical characterization using ESR spectroscopy for free radical detection and quantification, X-ray diffraction (XRD) for mineral type detection, and Fourier transform infrared (FTIR) for functional group analysis.

2.2.1. Electron Spin Resonance (ESR) Spectroscopy

The ESR was used to detect the presence of free radical species in the collected dust samples. A sample of dust was transferred into an ESR tube with the following characteristics: ESR5000 Sample tube P 135/3 made of synthetic quartz, measuring 150 mm in length, with an outer diameter of 3 mm and a wall thickness of 0.4 ± 0.1 mm. Care was taken to fill the ESR tube to the required level with the use of a Bruker Cavity Sampler to detect the sample effectively. Since ESR is a volumetric analysis, it was important to fill the recommended length of 3 cm in the tube and to center the sample properly for accurate measurement. This corresponded to around 2 g per run sample. The tube was then capped and placed into the Bruker Magnettech ESR5000 (Bruker, Billerica, MA USA), which operated at an X-Band frequency of 9.41 GHz for the measurement. The measurement took place in the magnetic field range between 308 and 368 mT, at a 100 kHz modulation frequency, and at 14.9 mW microwave power. Three replicates were taken per measurement with a scan time of 60 s per replicate. The free radical content was systematically analyzed and quantified through the embedded user interface software in the system (ESRstudio), which correlated to a sample of known free radical quantities, namely 2,2-diphenyl-1-picrylhydrazyl (DPPH) in toluene.

2.2.2. Fourier Transform InfraRed (FTIR)

The Jasco FTIR-4700 (Jasco, Tokyo, Japan) was used; the sample was placed on a plate inside the chamber of the equipment. From one side of the chamber, a beam of IR was directed at the sample. The sample particles absorbed some of the IR light, while the rest was transmitted through the sample. A detector at the opposite side of the chamber collected the transferred IR beam and measured it. The detector recorded more than 6000 single data points and constructed a spectrum on a 2D graph. These data were collected over the range of 400 cm^{-1} to 4000 cm^{-1}.

2.2.3. X-Ray Diffraction (XRD)

This characterization was performed using the X'Pert 3-XRD by Philip X Co. (Almelo, The Netherlands). XRD works by directing a beam of X-rays at the sample, then measuring the diffracted X-rays. The arrangement of atoms in the sample was determined from the measured X-ray diffraction data, with a 2θ range of 20–70°. The X-ray diffractometer operated at 40 kV and 30 mA, using Cu Kα radiation.

3. Results and Discussion

3.1. Detection and Quantification of Free Radicals in Dust

Free radicals, by definition, are entities that contain within their valence shell a free unpaired electron. That missing electron in their electronic configuration renders free radicals extremely reactive and unstable, with a tendency to abstract an electron to fulfill that absence. EPFRs, on the other hand, are free radicals that are persistent and not short-lived. The definition of persistent free radicals has been debatable. This issue was previously addressed, and the difference between persistence and stability of free radicals was discussed in work [43]. Nevertheless, when an electron is unpaired, it exhibits a magnetic spin, which, upon excitation by a magnetic field, "flips" to another spin state. This is exactly how the electron spin resonance spectroscopy (ESR) operates. When the spin "flips", the ESR is able to detect the absorbance, thus generating a peak. This makes the ESR an appropriate apparatus to detect the EPFRs [44,45]. ESR also detects paramagnetic species, in general, including transition metals. Nonetheless, the quantification and detection of free radicals are relatively complex processes. There are many factors that could play a role in these processes; e.g., the concentration must fall within a specific range to be above the

detection limit of the instrument [45]. The sample concentration must be high enough to be detected by the ESR, yet not too high to avoid incurring power saturation, a process that is found by trial and error. In addition, the solvent has a large impact on the free radical concentration [46–48]. For this reason, samples were collected without the use of any solvent. Moreover, an internal standard of known quantity is used as a reference for calibration in the software.

In the current study, the collected samples were tested using ESR spectroscopy, and the following ESR spectra were obtained (Figure 1).

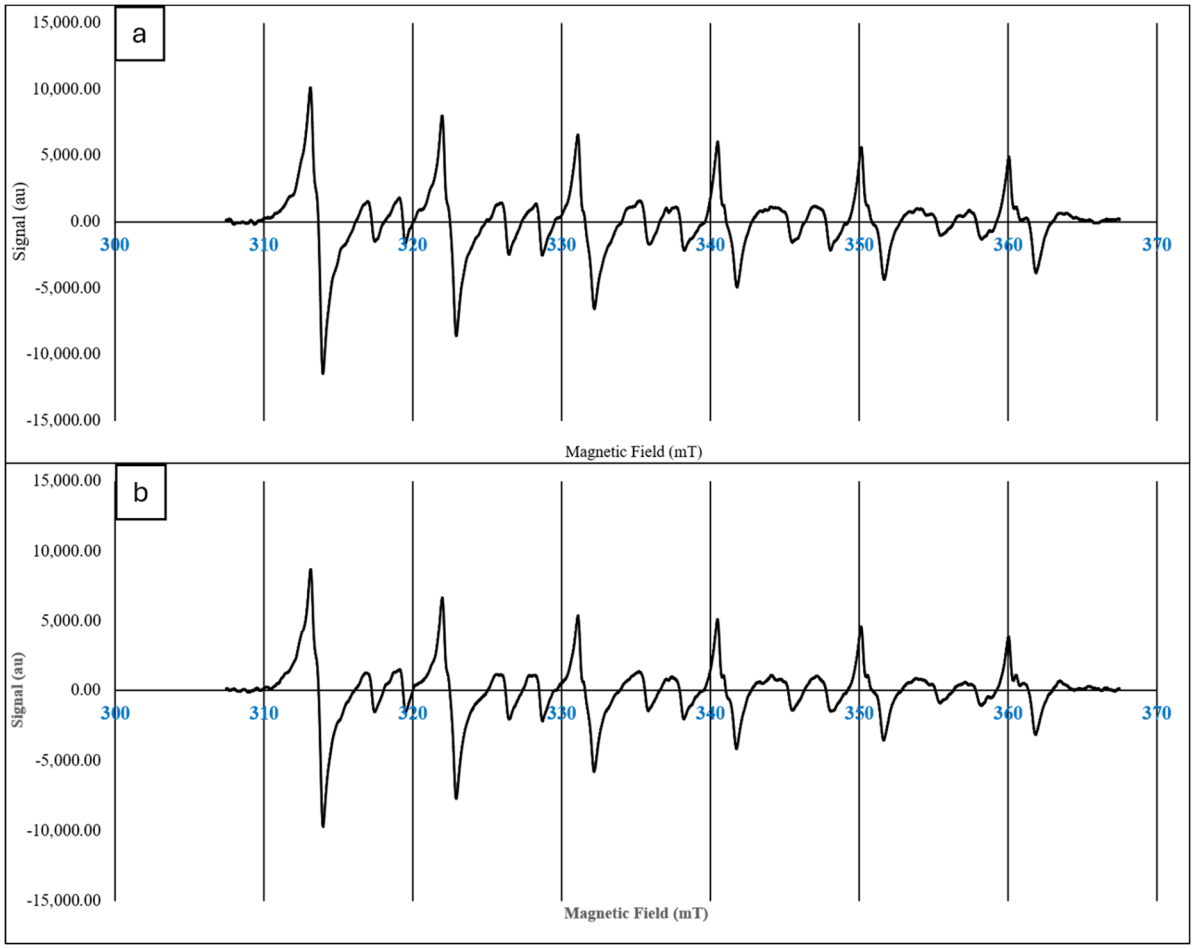


Figure 1. ESR spectra of samples collected from DS1 (**a**) and DS2 (**b**).

The presence of identifiable peaks suggests the detection of free radicals within the measured sample. It can be noted that both samples reported nearly identical spectra obtained using the ESR equipment, implying similar types of EPFRs in the dust tested. It can be observed that the peaks are well-defined with minimal noise, reflecting the large and well-defined amounts of free radicals present in our samples. Only a relatively limited number of studies have employed ESR to detect free radicals in aerosols. Yang et al. found no detectable ESR peaks for many of their tested samples, especially particulate matter of sizes above 1 μm [5]. This was justified by the greater availability of active and adsorption sites for EPFRs in smaller particles that are more porous.

Since EPFRs are classified as a type of pollutant, it is imperative to not only detect but also quantify the amount of free radicals found in a sample. It would then be compared with the environmental regulations to identify whether the levels comply with the recommended levels. The total number of detected free radical spins/g dust was 2.64×10^{16} and 2.36×10^{17} for DS1 and DS2 samples, respectively.

Shaltout et al. reported similar values, with an average of (1.6–5.8) $\times 10^{16}$ spins/g in the city of Taif in Saudi Arabia, while anticipating semiquinones as the prevalent type of EPFR [39]. In China, Yang et al. reported a higher average spins/g in a range between (2.63–19.4) $\times 10^{19}$ in Beijing, while a study by Wang et al. in Xuanwei, China showed it had a spins/g average of around 4.74 $\times 10^{18}$, and He et al. reported 1.353 $\times 10^{13}$ to 4.653 $\times 10^{13}$ spins/g in the city of Shihezi [5,42,49]. On the other side of the globe, studies by Squadrito et al. reported a lower average spins/g of EPFRs in Phoenix and Philadelphia, USA, at around (5 $\pm$ 0.8) $\times 10^{16}$, but still within similar values as our DS1 sample, and Gehling & Dellinger reported a range of 2.46 $\times 10^{16}$ to 2.79 $\times 10^{17}$ spins/g [18,40]. In India, where pollution is a major issue (as in China), Roy et al. reported that the EPFRs in PM in the city of Pune average around 10^{17}–10^{18} spins/g [41]. In Europe, where environmental standards are especially highly regarded, Arangio et al. and Filippi et al. reported an average spins/g of 7 $\times 10^{17}$ in the city of Mainz in Germany [33,50]. In Australia, Lee et al. reported median household dust EPFR concentrations of 1.65 $\times 10^{16}$ spins/g in one cohort and 5.78 $\times 10^{16}$ spins/g in the other [35].

3.2. Interpretation of the Possible Chemical Structures and Linkages

After using ESR to detect and quantify the total amount of free radicals present, the next step is to identify the type that was detected using the *g*-factor. This is then confirmed with the use of the X-ray diffraction apparatus, as well as the Fourier transform infrared spectroscopy. XRD is used to identify the metallic crystalline structures within the dust sample that could act as the surface on which these possible EPFRs can attach and persist. On the other hand, FTIR is used to identify the types of bonds present within the structure, which gives an idea of the linkages that should appear in a model structure of the EPFR being detected.

In order to distinguish between different types of free radicals, the intrinsic property known as the g-factor is used. This property is a dimensionless parameter mainly dependent upon the type of the free radical center as well as its neighboring atoms; i.e., the location and atom at which the free radical exists within the structure of the molecule [45]. It can be located by the intersection of the ESR spectrum with the *x*-axis. The magnetic field can be found and then converted into the effective *g*-factor according to the following Equation (1):

$$g = \frac{h \times \nu}{\mu_B \times B_0}, \quad (1)$$

In which g represents the g-factor, h denotes Planck's constant (6.626 $\times 10^{-34}$ J·s), ν is the microwave frequency of the ESR instrument in hertz (Hz), μ_B is the Bohr magneton (9.273 $\times 10^{-28}$ J/Gauss), and B_0 corresponds to the magnetic field measured in Gauss.

Typically, *g*-factors are within the ranges of 1.9 to 2.1, with the *g*-factor value of a free electron being 2.0023 [51]. On the other hand, carbon-centered free radicals usually result in a *g*-factor value less than 2.0030. In fact, the closer the free radical gets to an oxygen atom, the more the *g*-factor increases, with oxygen-adjacent carbon-centered free radicals incurring a *g*-factor in the range of 2.0030–2.0040, and oxygen-centered free radicals exhibiting *g*-factors greater than 2.0040 [52].

The effective *g*-factors of the spectra displayed in Figure 1, along with their corresponding magnetic field (B) values and peak-to-peak line width ($\Delta H_{P\text{-}P}$) are shown below in Table 1:

Table 1. *g*-factor, magnetic field (B), and peak-to-peak values for the peaks (left to right) presented in the ESR spectrum of DS1 in Figure 2.

***g*-factor**	**2.1526**	**2.0934**	**2.036**	**1.9799**	**1.9252**	**1.8709**
B (mT)	313.72	322.59	331.62	340.92	350.49	360.57
ΔH_{P-P} (Gauss)	8.426	9.546	11.078	13.089	15.641	18.642

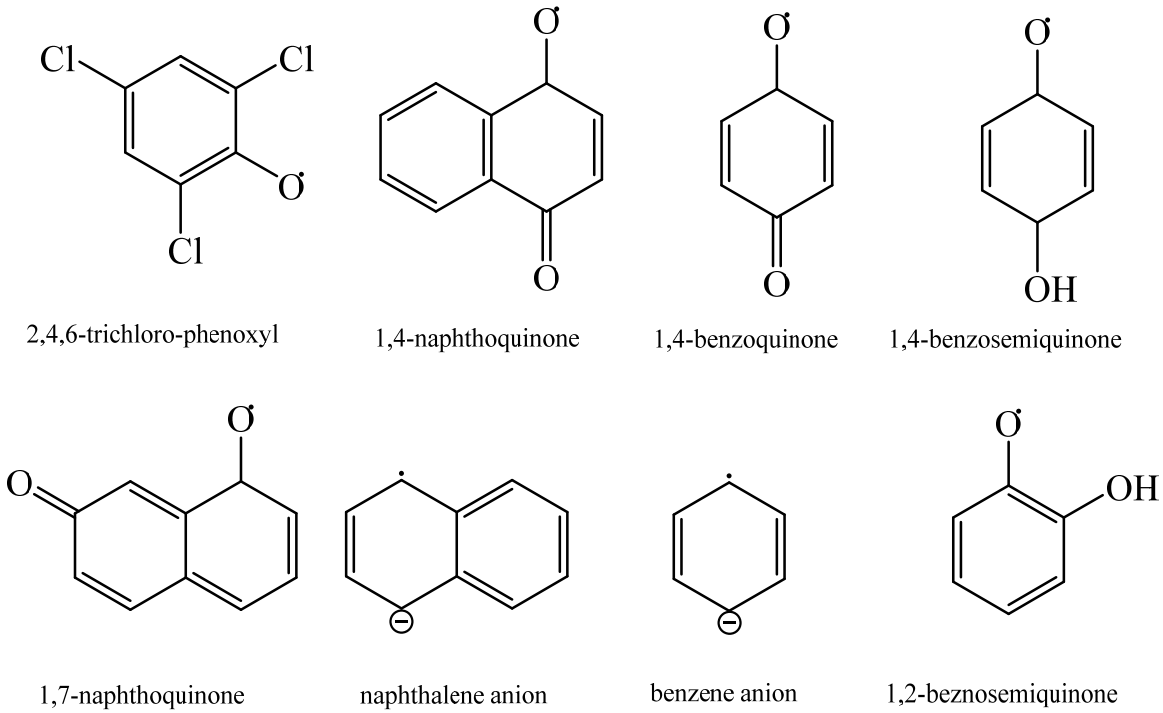


Figure 2. Possible EPFR structures.

The peak-to-peak linewidth seems to vary between all of the six peaks identified in the spectrum, with values ranging from 8.4 to 18.6 Gauss. In comparison, the ΔH_{P-P} of samples reported for different cities in the USA has a similar value, yet a smaller range, with values reported between 5 and 10.6 Gauss among the cities of Baton Rouge, Philadelphia, and Phoenix, USA [18,40,53]. Furthermore, in the city of Taif, Saudi Arabia, peak-to-peak linewidths of EPFRs were reported to range from 9.5 to 14.3 Gauss [39].

The variety of g-factor values, as well as their extended range, could suggest the presence of more than one type of free radical species being detected by the ESR. Nonetheless, the fact that the spectra are identical despite being taken from samples from totally distinct locations makes it highly unlikely. The spread of the spectrum over six widely spaced peaks might also indicate the predominant presence of manganese ions within the sample. In this case, what can be seen is both the allowed (i.e., the bigger, sharper peaks) and forbidden (i.e., the smaller peaks in between) transitions of the Mn^{2+} high-spin system [54,55].

Mn^{2+} in dust and soil samples is not uncommon, with studies linking its prevalent presence to an increase in multiple diseases such as Parkinsonism [56,57]. This usually occurs in places of current or historical presence of ferroalloy factories, which induce chronic environmental exposure [58]. This can cause a variety of detrimental health effects, such as impaired motor function as well as erratic behavior [59–61].

Mn^{2+} can also reach the soils through leaching from groundwater. As it is one of the most abundant metals in Earth's crust, it has a high tendency to infiltrate groundwater and reach soils, potentially leading to airborne transport into indoor dust [62]. Moreover, manganese can be spread through fungicides, which are typically used for agricultural

purposes. This would end up elevating the airborne levels, which can then be detected inside different homes in collected dust samples [63].

Nonetheless, this does not indefinitely preclude the presence of free radical entities of organic origin within the sample, yet their presence can be entirely masked by the Mn^{2+} due to a pronounced difference in concentrations.

The center value of the spectra in terms of the g-factor is around 2.004–2.006. This also corresponds to the g-value range of quinones and semi-quinones, typical free radical species that are found in EPFRs [64]. Typical EPFR structures are shown in Figure 2. Hyperfine splitting takes place in the case of the presence of neighboring atoms that have non-zero nuclear spin. It is well-established that the minute loads of transition metal oxides loaded on PM mediate the rupture of the phenolic O-H bond, leading to the formation of EPFRs [65]. Adsorbed phenolate structures are subsequently attached to the cation M^+ sites.

Since our samples existed in an open environment at high outdoor and indoor temperatures, typical of the UAE, for extended periods of time, this means they were susceptible to oxidation of the radical center. However, since the free radical was successfully detected and persisted for such a long period, it is more likely to be an oxygen-centered radical. In fact, radical reactivity with oxygen depends on the radical center: carbon-centered radicals are more reactive with oxygen and can form peroxides, while oxygen-centered radicals yield less stable ozonides or have minimal interactions with oxygen [19].

In order to get a clearer idea of the samples that are being tested, XRD and FTIR characterizations were performed.

XRD was targeted as it could help identify the metallic compounds found in the dust, which act as the surface on which the complexes form, which helps persist or propagate the free radicals. Representative XRD spectra of dust samples are depicted in Figure 3.

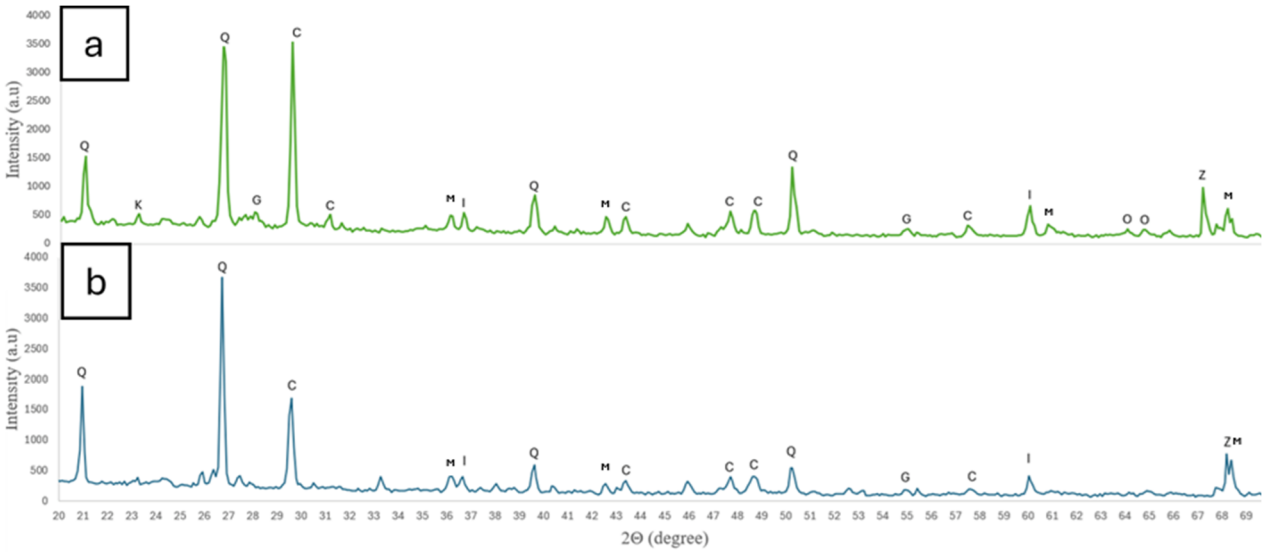


Figure 3. Representative XRD spectra for DS1 (**a**) and DS2 (**b**); Q denotes quartz, K denotes kaolinite, G denotes gypsum, C denotes calcite, M denotes anhydrite, Z denotes zincite, I denotes illite, and O denotes orthoclase.

Dust is typically a combination of many materials originating from various sources such as soil, road surface wear, biological inputs, and industrial activities. In addition, dust can be clearly affected by the geological factors related to the region. For instance, street dust is usually abundant in compounds such as Zn, Si, and Ca, which are represented by the minerals zincite, calcite, silica, and anhydrite (denoted by Z, C, Q, and A in Figure 3, respectively) and other metals such as illite, which is represented by I, and gypsum denoted

by G in Figure 3 [66]. Both samples showed the presence of Si, which is expected for the dry desert dust characteristic of the UAE. Also, calcium metal oxide was present in both samples in many forms, which is likely due to the carbonate content of regional sedimentary rocks.

On the other hand, it is observed from the comparison between the two samples that the peaks of DS2 are overall less intense compared to the peaks of DS1. The lower intensity of the DS2 peaks likely results from a combination of lower mineral abundance, smaller particle size, or poorer crystallinity.

Furthermore, the XRD results for DS2 indicate that there is no kaolinite or orthoclase (denoted by K and O in Figure 3) in the sample. The lack of these two minerals could be attributed to variations in source materials, weathering conditions, and local geology. More importantly, these measurements mainly prove the presence of metal sites that could act as the binders that facilitate the persistence of the EPFR, with copper, zinc, and aluminum known to act as oxidation-inducing catalytic sites, and that could, as a result, act as potent promoters of EPFR formation [67–70]. An example can be seen in Figure 4 below, which demonstrates the ability of copper to form a complex with different catechols, facilitating the persistence and binding of the free radicals to its surface. Aluminum is also known to form complexes with catechols, which are semiquinones and phenoxyl EPFR precursors [65,71].

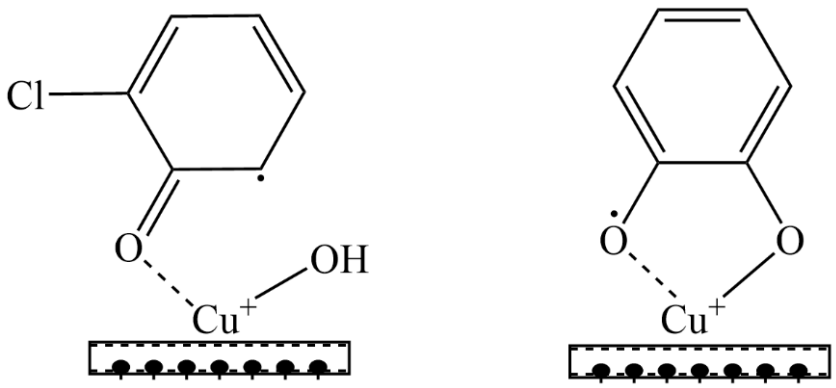


Figure 4. Examples of different metal–catechol complexes.

A summary of the descriptive statistics of major mineral percentages measured by XRD can be found below in Table 2.

Table 2. Summary of XRD peaks of dust samples DS1 and DS2.

Mineral	2 Θ	Sample	Reference
Quartz/Silica (SiO_2)	20.94°, 26.73°, 39.47°, 42.41°, 50.12°, 68.14°	DS1-DS2	[72,73]
Zincite (ZnO)	67.70°, 68.71°	DS1-DS2	[74]
Kaolinite ($Al_2O_3{\cdot}2SiO_2{\cdot}2H_2O$)	37.74°	DS1	[72,75]
Calcite ($CaCO_3$)	29.42°, 31.45°, 43.19°, 47.53°, 48.53°, 57.44°	DS1-DS2	[76,77]
Gypsum ($CaSO_4{\cdot}2H_2O$)	28.15°, 55.18°	DS1-DS2	[76,78]
Orthoclase $K(AlSi_3O_8)$	64.14°, 64.97°	DS1	[79]
Anhydrite ($Ca(SO_4)$)	31.39°, 36.31°	DS1-DS2	[80]
Periclase (MgO)	42.25°, 62.1°	DS1-DS2	[81,82]
Illite ($(K,H_3O)Al_2(Si_3Al)O_{10}(H_2O,OH)_2$)	35.51°, 60.05°	DS1-DS2	[83]

FTIR is a technique that has the ability to detect the presence of certain bonds, as well as their vibrations. This would help guide the thought process towards certain types of molecules present in the studied sample. Furthermore, functional groups can be identified

with the use of the FTIR, as well as the presence of heteroatoms such as halogens. Spectra obtained for the tested samples are presented in Figure 5.

Both samples showed very similar spectra in terms of FTIR peak positions, with some variations mainly taking place in terms of the transmittance. The overall results of the FTIR comply with the XRD results in terms of the existence of metals like Si, Al, and Ca, showing bonds that can be related to minerals such as quartz, calcites, as well as silicates. Table 3 below shows a summary of the FTIR peaks reported along with their tentative assignments in Figure 5.

Table 3. Summary of FTIR measurements for dust samples DS1 and DS2.

Functional Group	IR Frequencies (cm^{-1})	Tentative Assignment	References
Si–O bending vibration	1000–1160	Silicate minerals	[72]
Al–O coordination vibration and Si–O bending vibration	1650	NaAl silicate and CaAl silicate	[72]
Si–O symmetric bending; Si–O symmetric stretching	750, 900 and 1000–1150	Quartz	[72]
Asymmetric Stretching; CO_3 stretching; C = O and O–H stretching	870, 1420, 1350–1500, and 2550–2600	Calcite	[72]
Si–O deformation; O–H deformation; O–H stretching	800–900 and 1623	Kaolinite	[72]
C = C Stretching; N–H Bending	1470–1600	Aromatic compounds, catechols, or hydroquinones	[72,84,85]
C–H stretching vibrations	Around 2850	Typical for organic matter, suggesting the presence of hydrocarbons)	[72]
O–H stretching of water or alcohol; intramolecular hydrogen bonds	Broad 3300	moisture (water) in the soil, clay minerals (e.g., kaolinite), catechols	[72,84]
=C-H bending of an aromatic ring	810	Aromatics: catechols or hydroquinones	[84,85]
C-O vibrations	1250	Catechols or hydroquinones	[72,84,85]
Nitrate (NO_3^-)	1630	Organonitrates (R–O–N–O) aromatic amide, and amine organic functional groups	[72]
Sulphate (SO_4^{2-})	1090	Sulphate compounds	[72]

The combination of peaks reported at around 2850 and 3300 cm^{-1} is typical of organic substances, with the peaks at 810 and 1470–1600 cm^{-1} pointing more specifically to catechol or hydroquinone. The presence of these organic compounds that act as precursors to free radical semi-quinones validates the possibility of semi-quinones acting as the free radical entity detected by the ESR. Nonetheless, multiple different types of organic compounds that may exist in free-radical form can possibly be inferred from the data in Table 3, and not exclusively semi-quinones.

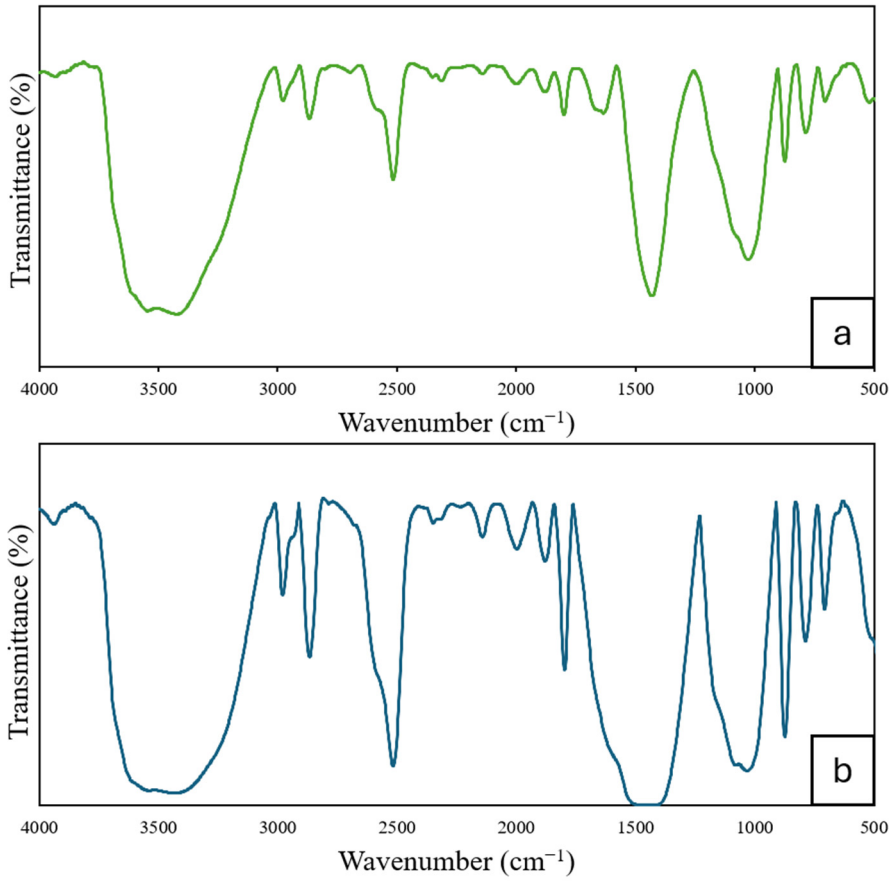


Figure 5. Representative FTIR of (**a**) DS1 and (**b**) DS2 dust samples in Al Ain, UAE.

4. Conclusions and Future Recommendations

This study investigated the presence and amount of free radical species in environmental dust collected from residential areas, using a solvent-free approach combined with ESR, XRD, and FTIR analyses.

The ESR spectra provided clear evidence of paramagnetic species. One of the major contributions of this study is the quantification of these species present in the dust samples belonging to two different areas, with DS1 and DS2 reporting 2.64×10^{16} and 2.36×10^{17} spins/g, respectively. These spin concentrations fall within the same order of magnitude as those reported in previous studies across different regions.

The interpretation of ESR peaks revealed the possibility that the signals reflect well-established environmentally persistent free radicals (EPFRs), particularly oxygen-centered radicals such as quinones or semiquinones. This interpretation is supported by the g-factor values near 2.004–2.006, which match well with reported ranges for these species. FTIR measurements reinforced this view, showing functional groups typical of catechols and hydroquinones—key precursors of EPFRs—while XRD confirmed the presence of mineral oxides that could stabilize such radicals on particle surfaces. This suggests that the dust samples indeed contain persistent organic radicals capable of generating oxidative stress and, therefore, pose potential health risks. Another explanation, however, is that the ESR signatures are primarily due to Mn^{2+} ions masking EPFRs. The spectra exhibit features consistent with manganese's characteristic six-line hyperfine splitting, including both allowed and forbidden transitions across a broad g-factor range. Given the natural abundance of manganese in desert dust and soils, its potential contribution from groundwater leaching or agricultural fungicides, and its well-established presence in environmental samples, this

is an equally strong and credible possibility. In this case, the manganese signals may either dominate the ESR response or even mask smaller contributions from organic radicals.

From a translational and commercialization perspective, these findings also suggest that solvent-free dust collection, combined with ESR-based quantification, could be developed as a specialized environmental testing and exposure screening service for homes, schools, workplaces, and industrial buffer zones, particularly in dust-prone arid regions such as the UAE. However, practical deployment would require standardized sampling and reporting protocols, larger seasonal and building-type validation datasets, quality assurance procedures, reference materials or interlaboratory comparisons, and careful separation of organic EPFR signals from inorganic paramagnetic interferences such as Mn^{2+}. Once these challenges are addressed, the approach could complement conventional PM monitoring by adding a chemical reactivity indicator and could support targeted mitigation actions, including improved filtration, ventilation management, cleaning practices, and source control decisions. Longer-term opportunities include standardized sampling kits, regional EPFR databases, and portable or semi-automated screening workflows for routine exposure assessment.

In conclusion, our results clearly show that dust samples contain paramagnetic species, which highlights potential health risks from exposure and calls for future research in this field.

Author Contributions: R.I.: Writing—original draft, visualization, validation, methodology, conceptualization, data curation, investigation. M.A.: writing—review and editing, conceptualization, resources, methodology. J.H.T.: writing—review and editing, visualization, supervision, resources, project administration, funding acquisition, conceptualization. All authors have read and agreed to the published version of the manuscript.

Funding: This study was supported by the Strategic Fund from the National Water and Energy Centre (NWEC) at the United Arab Emirates University (UAEU) [grant number: 12R157].

Data Availability Statement: The original contributions presented in this study are included in the article. Further inquiries can be directed to the corresponding author.

Conflicts of Interest: The authors declare no conflicts of interest.

References

1. Huang, L.; Zhou, L.; Chen, J.; Chen, K.; Liu, Y.; Chen, X.; Tang, F. Acute Effects of Air Pollution on Influenza-like Illness in Nanjing, China: A Population-Based Study. *Chemosphere* **2016**, *147*, 180–187. [CrossRef] [PubMed]
2. Du, Y.; Li, T. Assessment of Health-Based Economic Costs Linked to Fine Particulate (PM2.5) Pollution: A Case Study of Haze during January 2013 in Beijing, China. *Air Qual. Atmos. Health* **2016**, *9*, 439–445. [CrossRef]
3. Xu, P.; Chen, Y.; Ye, X. Haze, Air Pollution, and Health in China. *Lancet* **2013**, *382*, 2067. [CrossRef] [PubMed]
4. Jin, R.; Liu, G.; Jiang, X.; Liang, Y.; Fiedler, H.; Yang, L.; Zhu, Q.; Xu, Y.; Gao, L.; Su, G.; et al. Profiles, Sources and Potential Exposures of Parent, Chlorinated and Brominated Polycyclic Aromatic Hydrocarbons in Haze Associated Atmosphere. *Sci. Total Environ.* **2017**, *593–594*, 390–398. [CrossRef] [PubMed]
5. Yang, L.; Liu, G.; Zheng, M.; Jin, R.; Zhu, Q.; Zhao, Y.; Wu, X.; Xu, Y. Highly Elevated Levels and Particle-Size Distributions of Environmentally Persistent Free Radicals in Haze-Associated Atmosphere. *Environ. Sci. Technol.* **2017**, *51*, 7936–7944. [CrossRef] [PubMed]
6. Zhu, Q.; Liu, G.; Zheng, M.; Zhang, X.; Gao, L.; Su, G.; Liang, Y. Size Distribution and Sorption of Polychlorinated Biphenyls during Haze Episodes. *Atmos. Environ.* **2018**, *173*, 38–45. [CrossRef]
7. Particulate Matter ($PM_{2.5}$) Trends. US EPA. Available online: https://www.epa.gov/air-trends/particulate-matter-pm25-trends (accessed on 22 January 2025).
8. Organización Mundial de la Salud (OMS). *WHO Global Air Quality Guidelines*; World Health Organization: Geneva, Switzerland, 2021.
9. Yi, J.F.; Lin, Z.Z.; Li, X.; Zhou, Y.Q.; Guo, Y. A Short Review on Environmental Distribution and Toxicity of the Environmentally Persistent Free Radicals. *Chemosphere* **2023**, *340*, 139922. [CrossRef] [PubMed]

10. Health Effects Institute. *State of Global Air Report 2024*; Health Effects Institute: Boston, MA, USA, 2024. Available online: https://www.stateofglobalair.org/resources/archived/state-global-air-report-2024?utm_source=chatgpt.com (accessed on 29 June 2026).
11. Valavanidis, A.; Fiotakis, K.; Vlahogianni, T.; Papadimitriou, V.; Pantikaki, V. Determination of Selective Quinones and Quinoid Radicals in Airborne Particulate Matter and Vehicular Exhaust Particles. *Environ. Chem.* **2006**, *3*, 118–123. [CrossRef]
12. Khachatryan, L.; Vejerano, E.; Lomnicki, S.; Dellinger, B. Environmentally Persistent Free Radicals (EPFRs). 1. Generation of Reactive Oxygen Species in Aqueous Solutions. *Environ. Sci. Technol.* **2011**, *45*, 8559–8566. [CrossRef] [PubMed]
13. Zhang, X.; Chen, X.; Zhang, X. The Impact of Exposure to Air Pollution on Cognitive Performance. *Proc. Natl. Acad. Sci. USA* **2018**, *115*, 9193–9197. [CrossRef] [PubMed]
14. Kim, K.H.; Kabir, E.; Kabir, S. A Review on the Human Health Impact of Airborne Particulate Matter. *Environ. Int.* **2015**, *74*, 136–143. [CrossRef] [PubMed]
15. Guo, C.; Richmond-Bryant, J. A Critical Review of Environmentally Persistent Free Radical (EPFR) Solvent Extraction Methodology and Retrieval Efficiency. *Chemosphere* **2021**, *284*, 131353. [CrossRef] [PubMed]
16. Zhu, Q.; Zhang, X.; Dong, S.; Gao, L.; Liu, G.; Zheng, M. Gas and Particle Size Distributions of Polychlorinated Naphthalenes in the Atmosphere of Beijing, China. *Environ. Pollut.* **2016**, *212*, 128–134. [CrossRef] [PubMed]
17. Xu, Y.; Qin, L.; Liu, G.; Zheng, M.; Li, D.; Yang, L. Assessment of Personal Exposure to Environmentally Persistent Free Radicals in Airborne Particulate Matter. *J. Hazard. Mater.* **2021**, *409*, 125014. [CrossRef] [PubMed]
18. Gehling, W.; Dellinger, B. Environmentally Persistent Free Radicals and Their Lifetimes in PM 2.5. *Environ. Sci. Technol.* **2013**, *47*, 8172–8178. [CrossRef] [PubMed]
19. Dellinger, B.; Lomnicki, S.; Khachatryan, L.; Maskos, Z.; Hall, R.W.; Adounkpe, J.; McFerrin, C.; Truong, H. Formation and Stabilization of Persistent Free Radicals. *Proc. Combust. Inst.* **2007**, *31*, 521–528. [CrossRef] [PubMed]
20. Qin, L.; Zhu, W.; Yang, L.; Zheng, M.; Liu, G. Persistent Free Radicals in the Environment. *J. Hazard. Mater.* **2025**, *493*, 138332. [CrossRef] [PubMed]
21. Wang, X.; Liu, H.; Xue, Y.; Cui, L.; Chen, L.; Ho, K.F.; Huang, Y. Formation of Environmentally Persistent Free Radicals and Their Risks for Human Health: A Review. *Environ. Chem. Lett.* **2024**, *22*, 1327–1343. [CrossRef]
22. Xu, Y.; Lu, X.; Su, G.; Chen, X.; Meng, J.; Li, Q.; Wang, C.; Shi, B. Scientific and Regulatory Challenges of Environmentally Persistent Free Radicals: From Formation Theory to Risk Prevention Strategies. *J. Hazard. Mater.* **2023**, *456*, 131674. [CrossRef] [PubMed]
23. Chen, Q.; Wang, M.; Sun, H.; Wang, X.; Wang, Y.; Li, Y.; Zhang, L.; Mu, Z. Enhanced Health Risks from Exposure to Environmentally Persistent Free Radicals and the Oxidative Stress of PM2.5 from Asian Dust Storms in Erenhot, Zhangbei and Jinan, China. *Environ. Int.* **2018**, *121*, 260–268. [CrossRef] [PubMed]
24. Yang, L.; Liu, G.; Zheng, M.; Zhao, Y.; Jin, R.; Wu, X.; Xu, Y. Molecular Mechanism of Dioxin Formation from Chlorophenol Based on Electron Paramagnetic Resonance Spectroscopy. *Environ. Sci. Technol.* **2017**, *51*, 4999–5007. [CrossRef] [PubMed]
25. Jia, H.; Zhao, S.; Nulaji, G.; Tao, K.; Wang, F.; Sharma, V.K.; Wang, C. Environmentally Persistent Free Radicals in Soils of Past Coking Sites: Distribution and Stabilization. *Environ. Sci. Technol.* **2017**, *51*, 6000–6008. [CrossRef] [PubMed]
26. Gehling, W.; Khachatryan, L.; Dellinger, B. Hydroxyl Radical Generation from Environmentally Persistent Free Radicals (EPFRs) in PM2.5. *Environ. Sci. Technol.* **2014**, *48*, 4266–4272. [CrossRef] [PubMed]
27. Runberg, H.L.; Mitchell, D.G.; Eaton, S.S.; Eaton, G.R.; Majestic, B.J. Stability of Environmentally Persistent Free Radicals (EPFR) in Atmospheric Particulate Matter and Combustion Particles. *Atmos. Environ.* **2020**, *240*, 117809. [CrossRef]
28. Bitzer, Z.T.; Goel, R.; Reilly, S.M.; Foulds, J.; Muscat, J.; Elias, R.J.; Richie, J.P. Effects of Solvent and Temperature on Free Radical Formation in Electronic Cigarette Aerosols. *Chem. Res. Toxicol.* **2018**, *31*, 4–12. [CrossRef] [PubMed]
29. Vejerano, E.P.; Rao, G.; Khachatryan, L.; Cormier, S.A.; Lomnicki, S. Environmentally Persistent Free Radicals: Insights on a New Class of Pollutants. *Environ. Sci. Technol.* **2018**, *52*, 2468–2481. [CrossRef] [PubMed]
30. Pan, B.; Li, H.; Lang, D.; Xing, B. Environmentally Persistent Free Radicals: Occurrence, Formation Mechanisms and Implications. *Environ. Pollut.* **2019**, *248*, 320–331. [CrossRef] [PubMed]
31. Dela Cruz, A.L.N.; Gehling, W.; Lomnicki, S.; Cook, R.; Dellinger, B. Detection of Environmentally Persistent Free Radicals at a Superfund Wood Treating Site. *Environ. Sci. Technol.* **2011**, *45*, 6356–6365. [CrossRef] [PubMed]
32. Lomnicki, S.; Truong, H.; Vejerano, E.; Dellinger, B. Copper Oxide-Based Model of Persistent Free Radical Formation on Combustion-Derived Particulate Matter. *Environ. Sci. Technol.* **2008**, *42*, 4982–4988. [CrossRef] [PubMed]
33. Filippi, A.; Sheu, R.; Berkemeier, T.; Pöschl, U.; Tong, H.; Gentner, D.R. Environmentally Persistent Free Radicals in Indoor Particulate Matter, Dust, and on Surfaces. *Environ. Sci. Atmos.* **2022**, *2*, 128–136. [CrossRef]
34. Vilcins, D.; Dangal, P.; Lomnicki, S.; Cormier, S.A.; Lee, W.R.; Sly, P.D. Household Dust as a Reservoir for Environmentally Persistent Free Radicals: A Longitudinal Study. *Int. J. Environ. Health Res.* **2026**, *36*, 122–133. [CrossRef] [PubMed]

35. Lee, W.R.; Dangal, P.; Langan, G.; Lazarevic, N.; Xu, Z.; Cormier, S.A.; Lomnicki, S.; Sly, P.D.; Vilcins, D. Associations between Household Characteristics and Environmentally Persistent Free Radicals in House Dust from Two Australian Locations. *Front. Public Health* **2025**, *13*, 1603114. [CrossRef] [PubMed]
36. Li, H.; Chen, Q.; Wang, C.; Wang, R.; Sha, T.; Yang, X.; Ainur, D. Pollution Characteristics of Environmental Persistent Free Radicals (EPFRs) and Their Contribution to Oxidation Potential in Road Dust in a Large City in Northwest China. *J. Hazard. Mater.* **2023**, *442*, 130087. [CrossRef] [PubMed]
37. Fedorova, G.F.; Menshov, V.A.; Trofimov, A.V.; Tsaplev, Y.B.; Vasil'ev, R.F.; Yablonskaya, O.I. Chemiluminescence of Cigarette Smoke: Salient Features of the Phenomenon. *Photochem. Photobiol.* **2017**, *93*, 579–589. [CrossRef] [PubMed]
38. Belyakov, V.A.; Fedorova, G.F.; Vasil'ev, R.F. A Kinetic Chemiluminescence Study of the Antioxidants Evolved from Polymeric Materials into the Gaseous Phase. *J. Photochem. Photobiol. A Chem.* **1993**, *72*, 73–81. [CrossRef]
39. Shaltout, A.A.; Boman, J.; Shehadeh, Z.F.; Al-Malawi, D.A.; Hemeda, O.M.; Morsy, M.M. Spectroscopic Investigation of PM2.5 Collected at Industrial, Residential and Traffic Sites in Taif, Saudi Arabia. *J. Aerosol Sci.* **2015**, *79*, 97–108. [CrossRef]
40. Squadrito, G.L.; Cueto, R.; Dellinger, B.; Pryor, W.A. Quinoid Redox Cycling as a Mechanism for Sustained Free Radical Generation by Inhaled Airborne Particulate Matter. *Free Radic. Biol. Med.* **2001**, *31*, 1132–1138. [CrossRef] [PubMed]
41. Roy, R.; Jan, R.; Yadav, S.; Vasave, M.H.; Gursumeeran Satsangi, P. Study of Metals in Radical-Mediated Toxicity of Particulate Matter in Indoor Environments of Pune, India. *Air Qual. Atmos. Health* **2016**, *9*, 669–680. [CrossRef]
42. Wang, P.; Pan, B.; Li, H.; Huang, Y.; Dong, X.; Ai, F.; Liu, L.; Wu, M.; Xing, B. The Overlooked Occurrence of Environmentally Persistent Free Radicals in an Area with Low-Rank Coal Burning, Xuanwei, China. *Environ. Sci. Technol.* **2018**, *52*, 1054–1061. [CrossRef] [PubMed]
43. Yañez Jaramillo, L.M.; Tannous, J.H.; de Klerk, A. Persistent Free Radicals in Petroleum. *Processes* **2023**, *11*, 2067. [CrossRef]
44. Rozantsev, E.G.; Loshadkin, D.V. The History and Modern Problems of Free Radical Chemistry. 100 Years of Free Radical Chemistry. *Des. Monomers Polym.* **2012**, *4*, 281–300. [CrossRef]
45. Eaton, G.R.; Eaton, S.S.; Barr, D.P.; Weber, R.T. *Quantitative EPR*; Springer: Vienna, Austria, 2010.
46. Ismail, R.; Tannous, J.H. Investigation of the Free Radical Stability of 2,2-Diphenyl-1-Picrylhydrazyl upon Storage in Hydrogen- and Electron–Donning Solvents at Different Temperatures. *Case Stud. Chem. Environ. Eng.* **2025**, *11*, 101207. [CrossRef]
47. Tannous, J.H.; Tulegenova, D.; De Klerk, A. Effect of Solvents on Persistent Free Radical Content in the Absence of Reactions. *Energy Fuels* **2022**, *36*, 5253–5266. [CrossRef]
48. Almdallal, A.Q.; Ismail, R.; Tannous, J.H. Study on the Impact of Various Storage Conditions on the Free Radical Nature, Stability and Concentration of Oil. *Fuel* **2026**, *403*, 136081. [CrossRef]
49. He, F.; Lu, J.; Li, Z.; Li, M.; Liu, Z.; Tong, Y. Characteristics of Environmentally Persistent Free Radicals in PM2.5 and the Influence of Air Pollutants in Shihezi, Northwestern China. *Toxics* **2022**, *10*, 341. [CrossRef] [PubMed]
50. Arangio, A.M.; Tong, H.; Socorro, J.; Pöschl, U.; Shiraiwa, M. Quantification of Environmentally Persistent Free Radicals and Reactive Oxygen Species in Atmospheric Aerosol Particles. *Atmos. Chem. Phys.* **2016**, *16*, 13105–13119. [CrossRef]
51. Segal, B.G.; Kaplan, M.; Fraenkel, G.K. Measurement of g Values in the Electron Spin Resonance Spectra of Free Radicals. *J. Chem. Phys.* **1965**, *43*, 4191–4200. [CrossRef]
52. Khachatryan, L.; Adounkpe, J.; Dellinger, B. Formation of Phenoxy and Cyclopentadienyl Radicals from the Gas-Phase Pyrolysis of Phenol. *J. Phys. Chem. A* **2008**, *112*, 481–487. [CrossRef] [PubMed]
53. Dellinger, B.; Pryor, W.A.; Cueto, R.; Squadrito, G.L.; Deutsch, W.A. The Role of Combustion-Generated Radicals in the Toxicity of PM2.5. *Proc. Combust. Inst.* **2000**, *28*, 2675–2681. [CrossRef]
54. Murali, A.; Sreekanth Chakradhar, R.P.; Lakshmana Rao, J. Allowed and Forbidden Hyperfine Structure of Mn2+ Ions in Sodium Tetraborate Glasses—An EPR and Optical Study. *Phys. B Condens. Matter* **2005**, *358*, 19–26. [CrossRef]
55. Kliava, J.; Purans, J. Simulation of EPR Spectra of Mn^{2+} in Glasses. *J. Magn. Reson.* **1980**, *40*, 33–45. [CrossRef]
56. Olanow, C.W. Manganese-Induced Parkinsonism and Parkinson's Disease. *Ann. N. Y. Acad. Sci.* **2004**, *1012*, 209–223. [CrossRef] [PubMed]
57. Calne, D.B.; Chu, N.S.; Huang, C.C.; Lu, C.S.; Olanow, W. Manganism and Idiopathic Parkinsonism: Similarities and Differences. *Neurology* **1994**, *44*, 1583–1586. [CrossRef] [PubMed]
58. Pavilonis, B.T.; Lioy, P.J.; Guazzetti, S.; Bostick, B.C.; Donna, F.; Peli, M.; Zimmerman, N.J.; Bertrand, P.; Lucas, E.; Smith, D.R.; et al. Manganese Concentrations in Soil and Settled Dust in an Area with Historic Ferroalloy Production. *J. Expo. Sci. Environ. Epidemiol.* **2015**, *25*, 443–450. [CrossRef] [PubMed]
59. Martin, C.J. Manganese Neurotoxicity: Connecting the Dots along the Continuum of Dysfunction. *Neurotoxicology* **2006**, *27*, 347–349. [CrossRef] [PubMed]
60. Lee, J.W. Manganese Intoxication. *Arch. Neurol.* **2000**, *57*, 597–599. [CrossRef] [PubMed]
61. Zoni, S.; Bonetti, G.; Lucchini, R. Olfactory Functions at the Intersection between Environmental Exposure to Manganese and Parkinsonism. *J. Trace Elem. Med. Biol.* **2012**, *26*, 179–182. [CrossRef] [PubMed]

62. Liu, L.; Zhang, T.; Yu, X.; Mkandawire, V.; Ma, J.; Li, X. Removal of Fe^{2+} and Mn^{2+} from Polluted Groundwater by Insoluble Humic Acid/Tourmaline Composite Particles. *Materials* **2022**, *15*, 3130. [CrossRef] [PubMed]
63. Gunier, R.B.; Jerrett, M.; Smith, D.R.; Jursa, T.; Yousefi, P.; Camacho, J.; Hubbard, A.; Eskenazi, B.; Bradman, A. Determinants of Manganese Levels in House Dust Samples from the CHAMACOS Cohort. *Sci. Total Environ.* **2014**, *497–498*, 360–368. [CrossRef] [PubMed]
64. Xu, M.; Wu, T.; Tang, Y.T.; Chen, T.; Khachatryan, L.; Iyer, P.R.; Guo, D.; Chen, A.; Lyu, M.; Li, J.; et al. Environmentally Persistent Free Radicals in PM2.5: A Review. *Waste Dispos. Sustain. Energy* **2019**, *1*, 177–197. [CrossRef] [PubMed]
65. Altarawneh, M.; Assaf, N.W.; Hussain, H.M.; Dlugogorski, B.Z. Structural Properties of Alumina Surfaces and Their Roles in the Synthesis of Environmentally Persistent Free Radicals (EPFRs). *Nanotechnol. Rev.* **2023**, *12*, 20220536. [CrossRef]
66. Jassim, H.H.; Salman, I.M.; Al-Khafaji, R.M.N. Sedimentological and Heavy Metals Characteristics of Streets Dust in Some Areas East of Baghdad for 2020. *Iraqi Geol. J.* **2021**, *54*, 117–125. [CrossRef]
67. Ye, A.; Li, Z.; Ding, J.; Xiong, W.; Huang, W. Synergistic Catalysis of Al and Zn Sites of Spinel ZnAl2O4Catalyst for CO Hydrogenation to Methanol and Dimethyl Ether. *ACS Catal.* **2021**, *11*, 10014–10019. [CrossRef]
68. Sikora, F.J.; McBride, M.B. Aluminum Complexation by Catechol as Determined by Ultraviolet Spectrophotometry. *Environ. Sci. Technol.* **1989**, *23*, 349–356. [CrossRef]
69. Assaf, N.W.; Altarawneh, M.; Radny, M.W.; Al-Nu'Airat, J.; Dlugogorski, B.Z. Formation of Environmentally-Persistent Free Radicals (EPFR) on α-Al_2O_3 Clusters. *RSC Adv.* **2017**, *7*, 52672–52683. [CrossRef]
70. Ahmed, O.H.; Altarawneh, M.; Al-Harahsheh, M.; Jiang, Z.T.; Dlugogorski, B.Z. Formation of Phenoxy-Type Environmental Persistent Free Radicals (EPFRs) from Dissociative Adsorption of Phenol on Cu/Fe and Their Partial Oxides. *Chemosphere* **2020**, *240*, 124921. [CrossRef] [PubMed]
71. Gómez-Herrero, A.C.; Sánchez-Sánchez, C.; Chérioux, F.; Martínez, J.I.; Abad, J.; Floreano, L.; Verdini, A.; Cossaro, A.; Mazaleyrat, E.; Guisset, V.; et al. Copper-Assisted Oxidation of Catechols into Quinone Derivatives. *Chem. Sci.* **2021**, *12*, 2257–2267. [CrossRef] [PubMed]
72. El-Zahhar, A.A.; Idris, A.M.; Fawy, K.F.; Arshad, M. SEM, SEM-EDX, μ-ATR-FTIR and XRD for Urban Street Dust Characterisation. *Int. J. Environ. Anal. Chem.* **2021**, *101*, 988–1006. [CrossRef]
73. RRUFF Database. Quartz R100134. Available online: https://www.rruff.net/odr/rruff_sample#/odr/search/display/0/eyJkdF9pZCI6NzM4LCI3MDY5IjoiUjEwMDEzNCIsInNvcnRfYnkiOlt7InNvcnRfZGZfaWQiOiI3MDY5Iiwic29ydF9kaXIiOiJhc2MifV19 (accessed on 19 July 2026).
74. RRUFF Database. Zincite R050492. Available online: https://www.rruff.net/odr/rruff_sample#/odr/search/display/0/eyJkdF9pZCI6NzM4LCI3MDY5IjoiUjA1MDQ5MiIsInNvcnRfYnkiOlt7InNvcnRfZGZfaWQiOiI3MDY5Iiwic29ydF9kaXIiOiJhc2MifV19 (accessed on 19 July 2026).
75. RRUFF Database. Kaolinite R140004. Available online: https://www.rruff.net/odr/rruff_sample#/odr/search/display/0/eyJkdF9pZCI6NzM4LCI3MDY5IjoiUjE0MDAwNCIsInNvcnRfYnkiOlt7InNvcnRfZGZfaWQiOiI3MDY5Iiwic29ydF9kaXIiOiJhc2MifV19 (accessed on 19 July 2026).
76. Alraeesi, A.; Shah, A.H.; Hassan, A.; Laghari, M.S. Characterisation of Dust Particles Deposited on Photovoltaic Panels in the United Arab Emirates. *Appl. Sci.* **2023**, *13*, 13162. [CrossRef]
77. RRUFF Database. Calcite R050128. Available online: https://www.rruff.net/odr/rruff_sample#/odr/search/display/0/eyJkdF9pZCI6NzM4LCI3MDY5IjoiUjA1MDEyOCIsInNvcnRfYnkiOlt7InNvcnRfZGZfaWQiOiI3MDY5Iiwic29ydF9kaXIiOiJhc2MifV19 (accessed on 19 July 2026).
78. RRUFF Database. Gypsum R040029. Available online: https://www.rruff.net/odr/rruff_sample#/odr/search/display/0/eyJkdF9pZCI6NzM4LCI3MDY5IjoiUjA0MDAyOSIsInNvcnRfYnkiOlt7InNvcnRfZGZfaWQiOiI3MDY5Iiwic29ydF9kaXIiOiJhc2MifV19 (accessed on 19 July 2026).
79. RRUFF Database. Orthoclase R040055. Available online: https://www.rruff.net/odr/rruff_sample#/odr/search/display/0/eyJkdF9pZCI6NzM4LCI3MDY5IjoiUjA0MDA1NSIsInNvcnRfYnkiOlt7InNvcnRfZGZfaWQiOiI3MDY5Iiwic29ydF9kaXIiOiJhc2MifV19 (accessed on 19 July 2026).
80. RRUFF Database. Anhydrite R040012. Available online: https://www.rruff.net/odr/rruff_sample#/odr/search/display/0/eyJkdF9pZCI6NzM4LCI3MDUyIjoiXCJhbmh5ZHJpdGVcIiIsInNvcnRfYnkiOlt7InNvcnRfZGZfaWQiOiI3MDUyIiwic29ydF9kaXIiOiJhc2MifV19 (accessed on 19 July 2026).
81. Allan Nye, S.; Vineet, S.; Christopher, O.; Barnaby, S.; Chris, C. Use Of Olivine For The Production Of MgO-SiO_2 Binders. *Front. Built Environ.* **2021**, *7*, 640243. [CrossRef]
82. Harriman, A.; Siqueira, C.; Schons, A.B.; Appelt, P.; Silva, W.D.; Balaba, N.; Cunha, M.A.A.; Anaissi, F.J. Synthesis of Green Brucite [$Ni_xMg_{1-x}(OH)_2$] by Incorporation of Nickel Ions in the Periclase Phase (MgO) Applied as Pigments. *Colorants* **2024**, *3*, 138–151. [CrossRef]

83. RRUFF Database. Illite R180024. Available online: https://www.rruff.net/odr/rruff_sample#/odr/search/display/0/eyJkdF9pZCI6NzM4LCI3MDUyIjoiXCJpbGxpdGVcIiIsInNvcnRfYnkiOlt7InNvcnRfZGZfaWQiOiI3MDUyIiwic29ydF9kaXIiOiJhc2MifV19 (accessed on 19 July 2026).
84. Aktaş, N.; Şahiner, N.; Kantoğlu, Ö.; Salih, B.; Tanyolaç, A. Biosynthesis and Characterization of Laccase Catalyzed Poly(Catechol). *J. Polym. Environ.* **2003**, *11*, 123–128. [CrossRef]
85. Kafi-Ahmadi, L.; Javanpour, B. Synthesis and Characterization of New Binuclear Co(II) and Ni(II) Complexes Derived from N, N′-Bis(4-Dimethyl-Aminobenzylidene)-Benzene-1,3-Diamine as Active Catalysts for Hydroxylation of Phenol and Their Antibacterial Properties. *React. Kinet. Mech. Catal.* **2020**, *130*, 935–954. [CrossRef]

Disclaimer/Publisher's Note: The statements, opinions and data contained in all publications are solely those of the individual author(s) and contributor(s) and not of MDPI and/or the editor(s). MDPI and/or the editor(s) disclaim responsibility for any injury to people or property resulting from any ideas, methods, instructions or products referred to in the content.